LCLS-II Technical Note

THz wiggler design for the LCLS-II high-repetition rate facility

LCLS-II TN-21-06

APS-MD-TN-2021-002

9/30/2021

A.Fisher, M. Hoffmann, Z. Huang, A. Marinelli, M. Qian, S. Sasaki, J. Xu, Z. Zhang (SLAC and ANL)

1 Introduction

The effective coupling of advanced sources of terahertz (THz) radiation with an X-ray free-electron laser (XFEL) will open many new science opportunities. To match the high repetition rate of LCLS-II (up to 1 MHz), we have proposed a wiggler-based THz source that is driven by the same superconducting linac and hence provides accurate synchronization between THz and X-rays (Z. Zhang *et al*., 2020, Ref. [1]). The wiggler-based source is tunable between 3-20 THz with an energy of more than 100 µJ per pulse, independent of the accelerator's beam rate, and with a relatively narrow bandwidth to explore resonant excitations.

In this note, we discuss the physics requirements and designs for the THz wiggler proposed for high-rep. rate LCLS-II pump-probe experiments, and the expected THz radiation performance. The scientific motivation and preliminary design goals were laid out in Ref. [1]. Here we focus on the design of the THz wiggler that is compatible with LCLS-II-HE operation at 8 GeV.

2 Overview

A two-bunch scheme for the LCLS-II is used to produce a burst of intense THz radiation and an X-ray pulse with the adjustable time separation needed for pump–probe experiments, as shown in Figure 1. Two electron bunches with a suitable time delay are generated at the gun and sent through the linac. After acceleration to 8 GeV (following the HE upgrade), the beams are extracted and sent to the SXR line, where the XFEL undulator is followed by an eight-period wiggler that produces intense THz radiation. The THz wiggler is located between the SXR undulator and the beam dump. Since the THz pump must arrive earlier than the X-ray probe, the first bunch is used to produce a THz pulse while the second one lases in the FEL undulator. The initial time delay of the two beams compensates for the difference in the longer, less direct, transport path of the THz to the user station, compared with the nearly straight path of the X-rays.

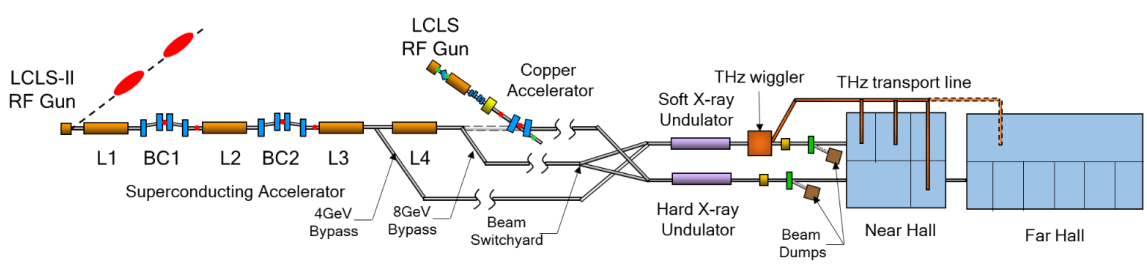

Figure 1: LCLS II layout showing the linac, fast kicker, soft and hard X-ray undulators, the proposed THz wiggler and transport line, and the Near and Far Experimental Halls.

3 General Wiggler Requirements

3.1 Wiggler parameters

We use the nominal beam energy (8 GeV) of the future LCLS-II high energy upgrade (LCLS-II-HE) to produce intense THz radiation through the proposed wigglers. The resonance equation determines the required effective magnetic field for different wiggler periods, as shown in Figure 2. A lower resonant frequency needs a higher magnetic field. The practical availability of the maximum magnetic field of an electromagnet (EM) wiggler led us to choose 140 cm as the wiggler period, where the maximum effective magnetic field of ~2 T matches a resonant frequency of 3

THz.

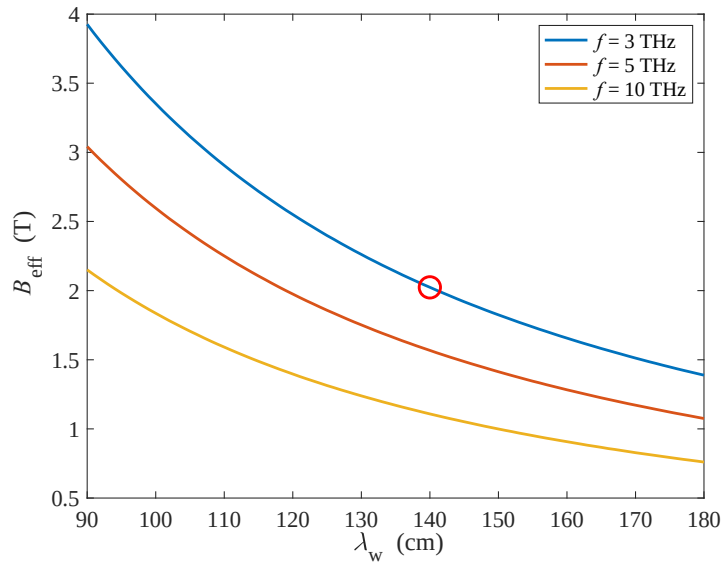

Figure 2 The effective magnetic field versus wiggler period at 3, 5 and 10 THz resonant frequency.

Table 1 presents the detailed parameters of the proposed EM wiggler with a 140-cm period. There are 8 periods in the wiggler, and its total length is 12.11 m in asymmetrical configuration including 14 regular poles and 4 corrector poles. This configuration is designed to allow the incoming and outgoing electron beam, and the emitted THz, to lie on the same axis. The field map of the asymmetrical configuration is shown in Figure 3. The wiggler gap of 50 mm is a trade-off between the maximum field requirement and the THz radiation output. In the EM wiggler, the magnetic field is varied by changing the current in the coils. To reach the 3 THz limit, the current in the coil is 306 A and the effective magnetic field is 2.03 T. Note that this effective field was calculated by keeping the first harmonic of the Fourier coefficients. The magnetic field and the effective field of a single regular period are presented in Figure 4. The field rolls off by 0.1% from the peak over a transverse distance of ± 10 mm in x, the direction of oscillation. Table 2 shows examples of current in the coils, the effective magnetic field, and the corresponding resonant frequency of the proposed EM wiggler.

Table 1: THz EM wiggler parameters for 8 GeV electron beam (140-cm period)

Parameter	Symbol	Nominal Value	Range	Unit
Electron beam energy	E	8		GeV
Wiggler type	-	Planar		-
Wiggler period	λ_w	140		cm
Number of full periods (excluding end poles)	N_w	8		-
Total wiggler length	L_w	12.11		m
Wiggler magnet type	-	EM		-
Magnet material	-	Iron with Cu coil		-
Wiggler full gap	g	50		mm

Parameter	Symbol	Nominal Value	Range	Unit
Radiation frequency	f_r	10	3-20	THz
Radiation wavelength	λ_r	30	15-100	μm
Wiggler strength parameter	K	145	102-265	-
Wiggler magnetic field strength	B	1.11	0.78-2.02	T
Wiggle strength tolerance	$\Delta K/K$ (rms)	<1%		-
Tuning good field range	r	± 10 @0.1%		mm
Field field intergral of B_y per cell	I_{1y}	$< 50 \times 10^{-4}$		Tm
Field field intergral of B_x per cell	I_{1x}	$< 50 \times 10^{-4}$		Tm
Second field intergral of B_y per cell	I_{2y}	$< 100 \times 10^{-4}$		Tm^2
Second field intergral of B_x per cell	I_{2x}	$< 100 \times 10^{-4}$		Tm^2

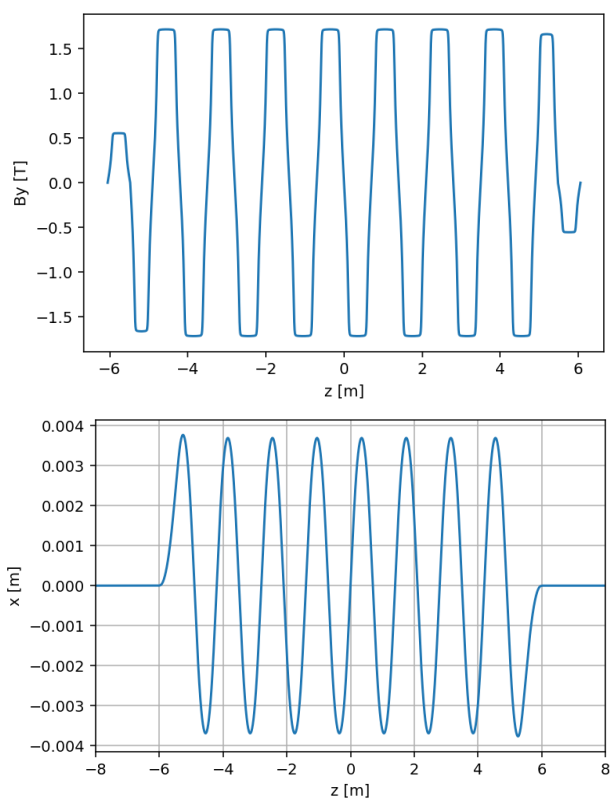

Figure 3: Asymmetrical configuration (14 regular poles and 4 corrector poles) with 12.11 m (left) and the corresponding beam trajectory whose incoming and outgoing lie on the same axis.

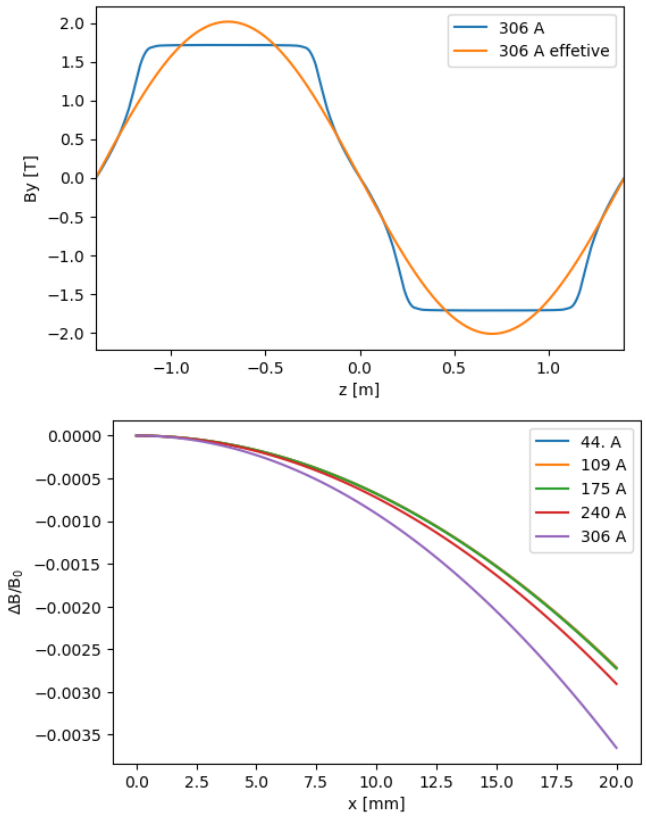

Figure 4: Magnetic field of single regular pole design (left) and field roll-off (right). Peak field 1.7T and effective peak field 2.03T for resonant frequency of 8GeV at 3THz.

Table 2: Current in coils, effective magnetic field, K and resonant frequency of the proposed THz EM wiggler (8 GeV and $\lambda_w = 140\text{cm}$).

Current (A)	Beff (T)	K	f_r (THz)
79.86	0.5541	72.45	40
113.05	0.7837	102.48	20
130.74	0.9050	118.34	15
160.43	1.1084	144.94	10
227.90	1.5676	204.97	5
306.40	2.0237	264.62	3

The field integrals determine the overall effect of the wiggler on the electron beam. The exit kick and position of the beam are given by

$$x'_{exit} = -\frac{I_{1x}}{B\rho}$$

$$y'_{exit} = \frac{I_{1y}}{B\rho}$$

$$x_{exit} = -\frac{I_{2x}}{B\rho}$$

$$y_{exit} = \frac{I_{2x}}{B\rho}$$

where $I_{1x,y}$ and $I_{2x,y}$ are the first and second field integral of the wiggler. $B\rho$ is the magnetic rigidity and can be obtained by $B\rho[Tm] = 3.3356E_e[GeV]$. With the requirements for beam orbit control, we can achieve the requirements for the field integral of the wiggler.

3.2 Field roll-off and pole surface shaping

According to the previous experience of XLEAP wiggler, the field roll-off of a wiggler along the direction of beam oscillation will introduce strong vertical focusing and horizontal defocusing effects on the beam. The proposed EM wiggler will shape the surface of the magnet poles to reshape the field roll-off and so reduce the focusing effects. Figure 5 shows the simulated field roll-off in the horizontal (x) direction without and with shaped pole surfaces. For the highest field, 2.03 T, the field drops by 0.034% at an offset of x = $\pm$10 mm, compared to an oscillation amplitude at this field strength of about ±7 mm. Shaping the pole surfaces reduces the field change to < 0.5e-4 at an offset of x = $\pm$10 mm. The reduced field roll-off makes the focusing effects much smaller, and it is easier to control the beam orbit.

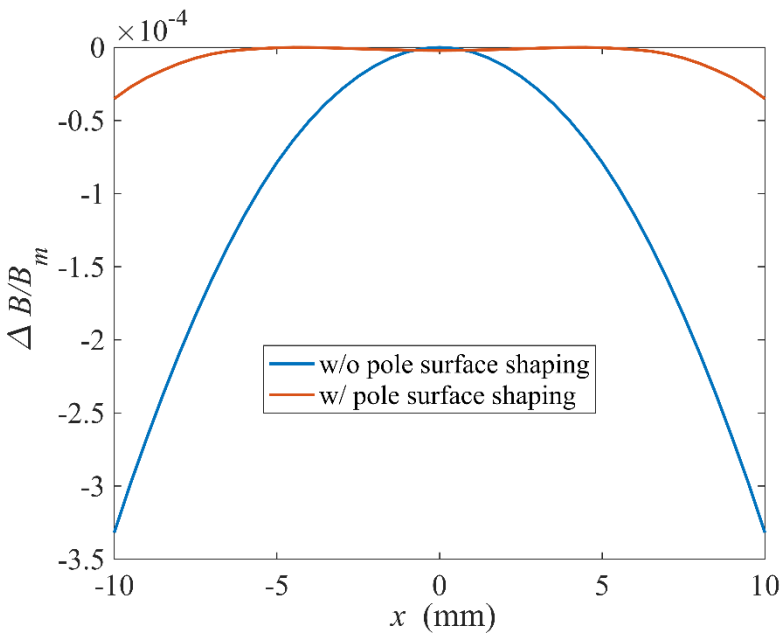

Figure 5: Roll-off of the wiggler field versus the horizontal offset from x = 0 at the center of the pole wihtout and with pole surface shaping.

3.3 Radiation damage and cooling requirements

In the proposed design of THz wiggler, the force between opposing poles is 73.6 kN, or 147 kN per period for the maximum current of 306 A. The temperature rise at this current is approximately 12°C. The conductor cross-section is 10 mm x 10 mm with a 5 mm-diameter water hole; a water pressure of 0.62 MPa is assumed. Each pole is surrounded by one coil, each coil has 117 turns of conductor. Each coil has three separate cooling-water loops. The power dissipated in each coil at 306 A is 9.2 kW. Since the THz wiggler is placed at the end of the undulator hall, the effects of this additional heat load on upstream HXR/SXR can be kept to minimum.

3.4 Beamline layout

The THz wiggler is located between the SXR undulator and the beam dump. Figure 6 shows the SXR and HXR undulator lines of the LCLS-II with cell numbers. LCLS-II-HE SXR undulator modifications will take up all space before Cell 26. The 3 DELTA-II undulators (for soft X-ray polarization control) can occupy Cell 45-47 since they can work in the horizontal polarization to provide the same functionality as SXR undulators. The beamline layout between the exit of the last SXR undulator and X-band deflector cavity (XTCAV) is presented in Figure 7. There is ~24m free space available for the THz wiggler and the THz mirror that decouples the radiation from the electron bunch. Another pump-probe experiment called PEPEX can be relocated after the THz wiggler to take advantage of the broad tunability of the THz wiggler for optical or even UV pump when the wiggler K is strongly reduced.

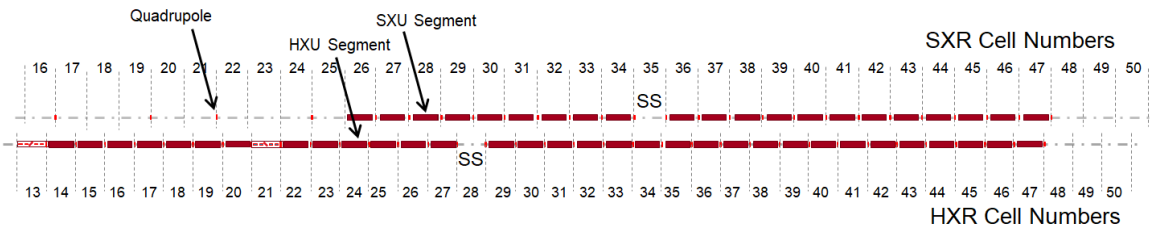

Figure 6: LCLS-II SXR and HXR undulator lines

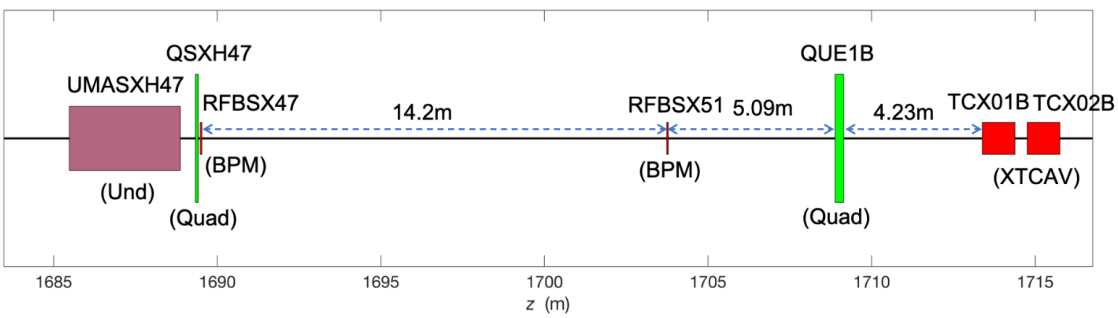

Figure 7: LCLS-II beamline layout between the SXR undulator and X-band deflector cavity (XTCAV).

3.5 THz mirror and transport line

THz emission from the body of the wiggler (as opposed to the transition undulator radiation (TUR) from its ends) is extracted by a mirror 10 m downstream from the middle of the wiggler (approximately 4 m from the end) and at 45° to the beam direction. At this distance, the emission has spread out sufficiently to allow a central hole large enough to safely pass the electrons but small enough to lose little THz power (see Figure 13). The mirror is oriented to direct this light horizontally, perpendicular to the beam. Both the mirror and hole are elliptical, but when seen from the wiggler projected onto the transverse plane, the mirror and central hole appear circular, with diameters of 100 mm and 10 mm respectively. Figure 13 shows that these diameters extract the wiggler radiation but pass much of the TUR through the hole. To avoid any reflection or diffraction from the beampipe, its inner diameter must be somewhat larger, widening to 150 mm between the wiggler exit and the mirror.

Figure 11 shows a maximum pulse energy of ~120 µJ at 10 THz on the mirror for a 200-pC electron bunch. The second electron bunch, for the X-ray FEL pulse, is 100 pC. At 8-GeV, the limit on power at the electron beam dump, 250 kW, restricts the rate for 300 pC to 100 kHz. At this rate, the

power on the mirror is 12 W. The total incoherent synchrotron radiation power generated by the wiggler is estimated to be 50 W (300 pC at 100 kHz). In vacuum, this power requires modest cooling that can be managed by conduction to a water-cooled support. We will model the thermal performance of a mirror with a Glidcop substrate and a gold coating, mounted on a support with a central water channel.

The THz transport line is evacuated to eliminate water vapor, which absorbs THz power. To protect the integrity of the beamline vacuum, the transport vacuum is separated by a window. The window material must be transparent throughout the frequency band of interest. Synthetic diamond (by chemical vapor deposition) is excellent and offers the advantage of also transmitting a visible alignment beam, but cost limits the maximum diameter to 50 mm. To accommodate this limit, we place the window at the first focal waist in the transport line.

Silicon windows are a common alternative for THz, since they are less expensive and available in larger diameters. However, silicon exhibits pronounced multi-phonon absorption peaks between 11 and 16 µm, limiting part of the intended wavelength range of 15 to 100 µm (3 to 20 THz).

The refractive index of diamond at these frequencies, 2.41, leads to large Fresnel reflection losses for normal incidence, reducing the transmission through the two surfaces to 70%. Since the wiggler emits linearly (horizontally) polarized light, these losses could be prevented by tilting the window at Brewster's angle. However, this angle is a steep 67.5° for this index, increasing the size of the window to an unrealistic 130 mm. Instead, we retain normal incidence but etch a robust "moth-eye" anti-reflection pattern onto the each surface, raising the transmission of a diamond window to 96%.

The transport line goes from the Undulator Hall to the Near Experimental Hall (NEH), where it can be directed to various user hutches. The transport path continues through the the X-Ray Tunnel (XRT) for other experiments requiring THz in the Far Experimental Hall (FEH).

The electron beam dump (EBD), which follows the Undulator Hall has an access "maze" running to the NEH. The maze provides a convenient path through the shielding for the THz transport line (Figure 8). This layout, with several 90° bends, is well suited to a "mirror guide" transport using multiple relay-imaging stages with off-axis parabolic (OAP) or toroidal mirrors. For coarse adjustment of the time difference between the THz and x ray pulses at a user experiment, the time interval between the two photocathode laser pulses can be shifted in increments of a gun RF period. For scans over shorter intervals, an "optical trombone" in the maze adjusts the optical path length. A second trombone next to the wiggler adjusts the focus at the launch of the transport line.

The many bends in a mirror guide make it less suited to the long (200 m) and straight path from NEH to FEH A cylindrical tube with periodic irises, acting as a wave guiding structure (an "iris line") has been proposed by DESY. In preparatory work, shorter lengths of the mirror guide and the iris line will be built and fully characterized experimentally, as shown in Figure 9.

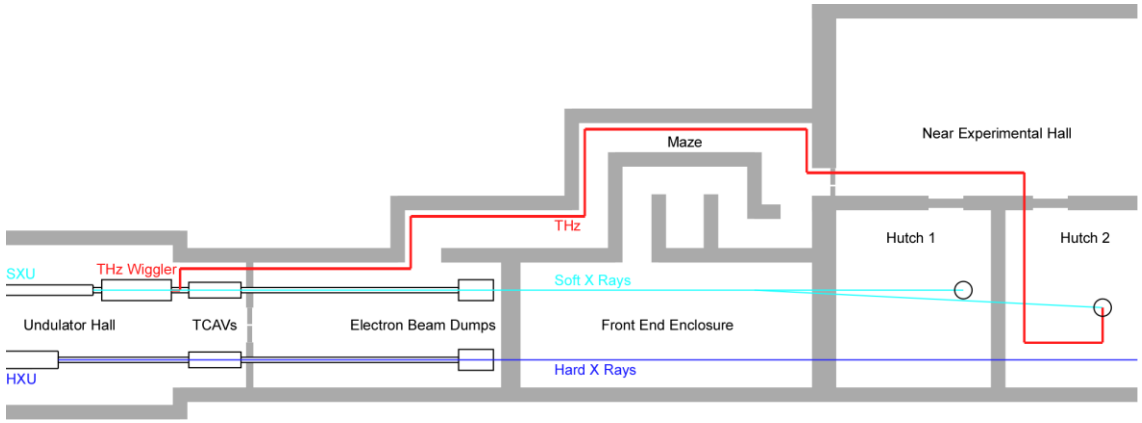

Figure 8 A simplified layout of the THz path from the Undulator Hall through the access maze to a user hutch in the Near Experimental Hall.

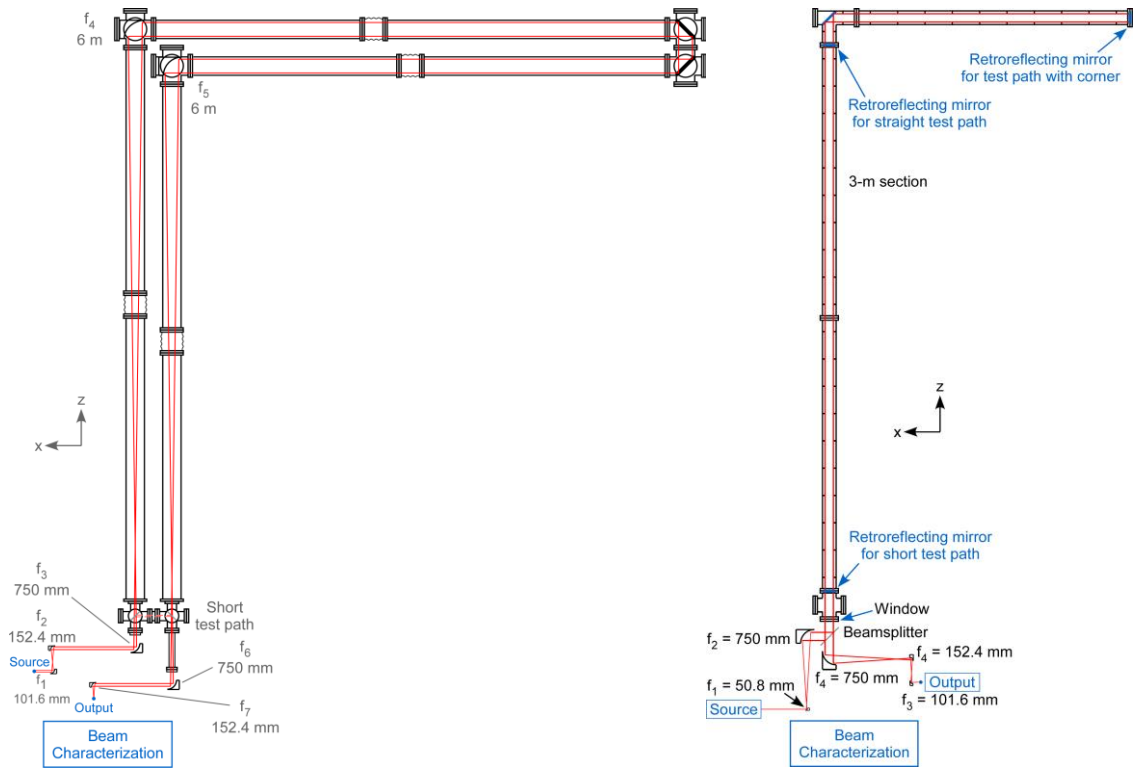

Figure 9 Setups planned for testing (a) the mirror guide and (b) the iris line.

4 Beam Optics Requirements

4.1 Beam optics

The proposed EM wiggler is located between the SXR undulators and X-band deflecting cavity (XTCAV). The design optics of this area are presented in Figure 10. The two dashed lines in the figure represent the positions of the wiggler. In order to study the effects on beam optics due to the wiggler, we can calculate the transfer matrix of the wiggler through particle tracking and then study its (de)focusing effects on the beam.

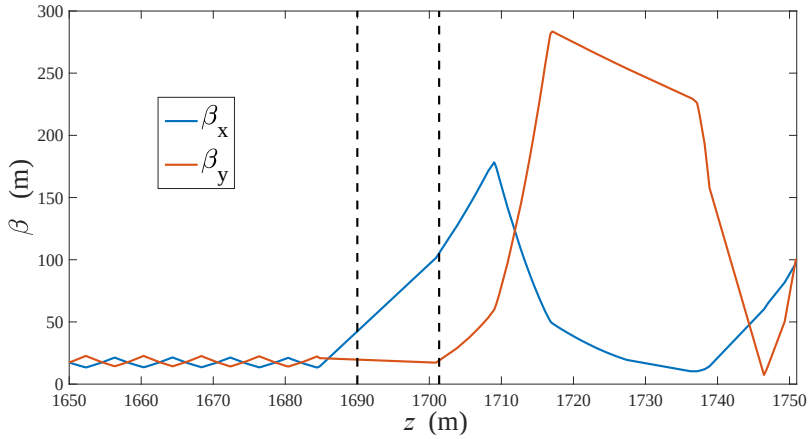

Figure 10 Beam lattice from undulators to beam dump. The two dashed lines represent the entrance and exit of the proposed EM wiggler.

4.2 Beam trajectory

In the proposed EM wiggler, the asymmetrical configuration of the trajectory guarantees the transverse overlapping of the radiation and the electron bunch when the undulator K is changed. No extra correctors are needed.

4.3 Focusing effects of the THz wiggler

The THz wiggler may have strong horizontal defocusing and vertical focusing due to the field roll-off and its natural focusing. We use a transfer matrix to describe the focusing effects of the proposed EM wiggler. The elements of the matrix can be calculated as a perturbation of the beam trajectory, similar to that adopted in the studies of XLEAP wigglers.

$$M_w = \begin{pmatrix} \Delta x_f/\Delta x_i & \Delta x_f/\Delta x_i' \\ \Delta x_f'/\Delta x_i & \Delta x_f'/\Delta x_i' \end{pmatrix}$$

For 8 GeV beam, the transfer matrix of the THz wiggler at maximum field can be written as

$$M_{w,x} = \begin{pmatrix} 1.0810 & 11.7317 \\ 0.0137 & 1.0817 \end{pmatrix} \quad \text{w/o pole surface shaping}$$

$$M_{w,x} = \begin{pmatrix} 1.0341 & 11.5525 \\ 0.0048 & 1.0315 \end{pmatrix} \quad \text{w/ pole surface shaping}$$

The transfer matrix for vertical plane (y) can be obtained by the same method with the horizontal magnetic field component B_x.

The natural focusing on the vertical plane can be calculated based on the resonance frequency. We take the maximum field (which is resonant at 3 THz) as an example. The focusing strength can be written as $K_q = \left(\frac{Kk_u}{\sqrt{2\gamma}}\right)^2$ and the corresponding transfer matrix will be

$$M_{w,y} = \begin{pmatrix} 0.8249 & 10.5283 \\ -0.0303 & 0.8249 \end{pmatrix}.$$

We can find that when there is no surface shaping, the defocusing effect in the horizontal plane induced by the field roll-off is smaller than the natural focusing of wiggler in the vertical plane.

The main focusing effect on electron beam from the proposed wiggler comes from its natural focusing with large K strength.

4.4 Focusing compensation by quadrupoles

From the transfer matrix of the EM wiggler calculated from the simulated magnetic field, the focusing effect is weak, which can be compensated directly by adjusting quadrupoles nearby. We will repeat the calculation of the transfer matrix with the measured magnetic field. Weak focusing can be compensated by tunning the quadrupoles after the undulators. However, if the focusing is strong due to imperfections in the magnetic field, we can install a new quadrupole close to the wiggler for compensation.

5 THz Radiation Calculation

5.1 THz pulse energy

The total achievable THz pulse energy depends on the specific layout of the wiggler and transport system (THz mirrors). Here we can estimate the pulse energy by the bunching factor spectra and the simplified equation for the single-electron radiated energy into the central cone, defined as $\theta_c \simeq K/(\gamma\sqrt{N_w})$,

$$W_1 = 1.431 \times 10^{17} ehv \frac{d\omega}{\omega} \frac{K^2[JJ]_1^2}{1+K^2/2} ,$$

where $e = 1.6 \times 10^{-19}$ C is the elementary charge, $h\nu$ is the radiated photon energy and $d\omega/\omega$ is the bandwidth of interest. The Bessel function factor

$$[JJ]_1 = J_0\left(\frac{K^2}{4+2K^2}\right) - J_1\left(\frac{K^2}{4+2K^2}\right).$$

The total pulse energy can be written as

$$W = W_1 N_w \left(\frac{Q}{e}\right)^2 b(\nu)^2.$$

Here N_w is the number of wiggler periods, Q is the beam charge, and $b(\nu)$ is the bunching factor at the radiation frequency b(v) = 1-0.019 f [THz].

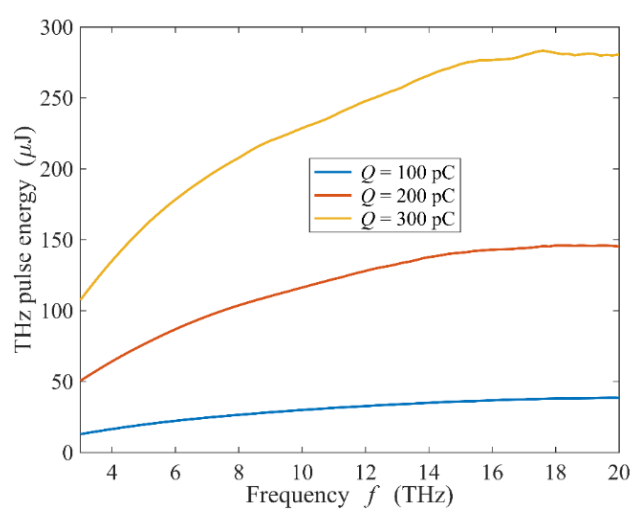

Figure 11: The estimated THz pulse energy of different beams versus the radiation frequency.

5.2 THz radiation distribution and spectra

The THz radiation from the wiggler is calculated by the code developed by one of the authors, M. Qian. The THz spectra and its transverse distribution with a hole at the center radiated by an 8-GeV electron beam are presented in Figure 12 and Figure 13, at K= 264.62 for the fundamental frequency of 3 THz. At 9 THz (the third harmonic) and assuming a 10% bandpass filter, the THz pulse energy is about 200 µJ for a 200-pC fully bunched beam. The beam dynamics [1] suggests the bunching factor is $1 - 0.019f[\mathrm{THz}] = 0.83$ for 9 THz, so the total pulse energy over a 10% BW is 130 µJ.

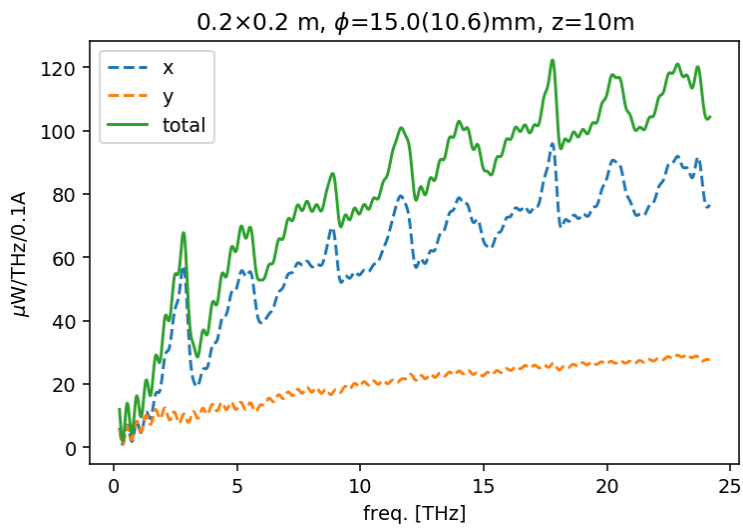

Figure 12: Radiation spectra of 8 GeV electron beam resonant at 3 THz in the asymmetrical configuration.

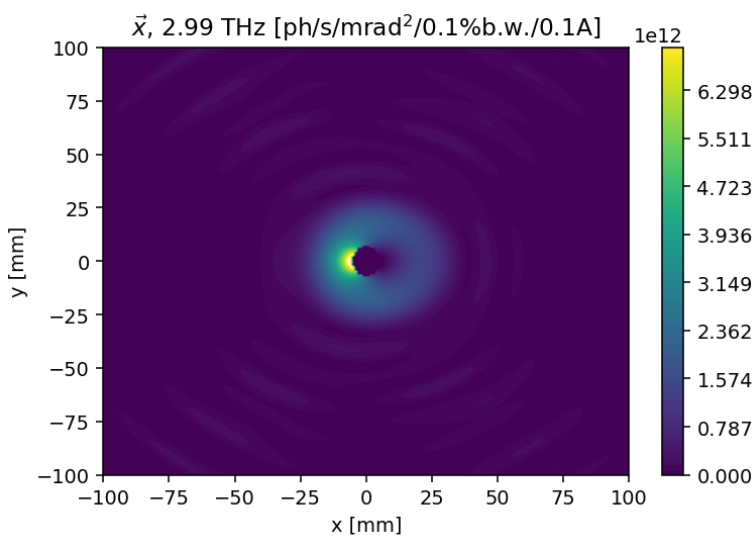

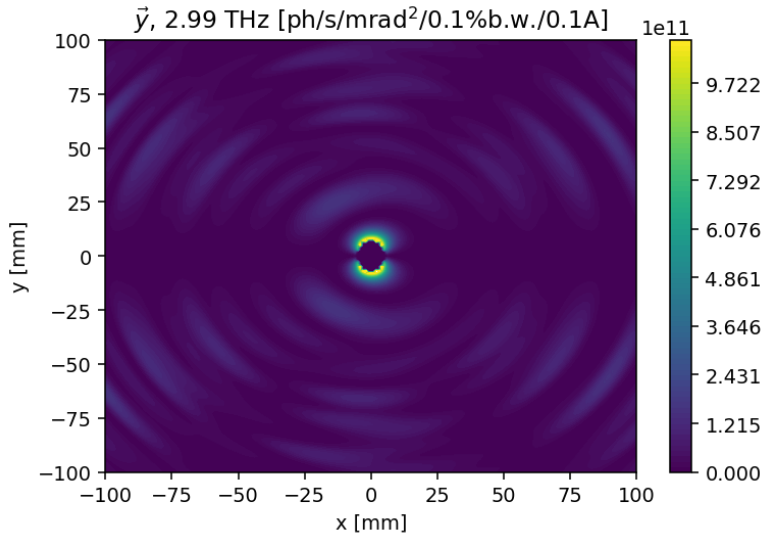

Figure 13: THz radiation transverse distribution at Z = 10 m in the asymmetrical configuration.

5.3 Transition undulator radiation

The two edges of the wiggler itself produce edge radiation. They interfere with each other and make transition undulator radiation (TUR). In our case, the electron beam passes through the hole in the center of the 45° reflecting mirror. This configuration contributes to the near field radiation at the THz range too.

To handle this complicated configuration, we developed a calculation code to simulate THz radiation from near field radiation of the beam, the TUR as well the normal undulator radiation. The code is based on the classic formula:

$$\frac{d^2I}{dA} = \frac{\alpha}{4\pi^2}\frac{\Delta\omega}{\omega}\left|\int_{-\infty}^{+\infty}\left\{\frac{c(\boldsymbol{n}-\boldsymbol{\beta})}{R^2\gamma^2(1-\boldsymbol{n}\cdot\boldsymbol{\beta})^3}+\frac{\boldsymbol{n}\times\left((\boldsymbol{n}-\boldsymbol{\beta})\times\dot{\boldsymbol{\beta}}\right)}{R(1-\boldsymbol{n}\cdot\boldsymbol{\beta})^3}\right\}_{t'} e^{i\omega t(t')}\,dt'\right|^2$$

Where I and A are the flux density and the unit surface area of the observing plane, ω is the radiation angular frequency, $\boldsymbol{R} = \boldsymbol{n}R$ is the vector pointing from the electron to the observing point. The trajectory of the electron passing through the undulator is calculated first and divided into 10^5 segments. The $\boldsymbol{\beta}$ and $\boldsymbol{R}$ of each segment are put into the above formula and the output from which is integrated over all segments to give the flux density at the observing plane. In Figure 14 we present the calculated spectra of on-axis undulator radiation and off-axis ($\theta_x = 0.06\text{mrad}, \theta_y = 0$) TUR for comparsion.

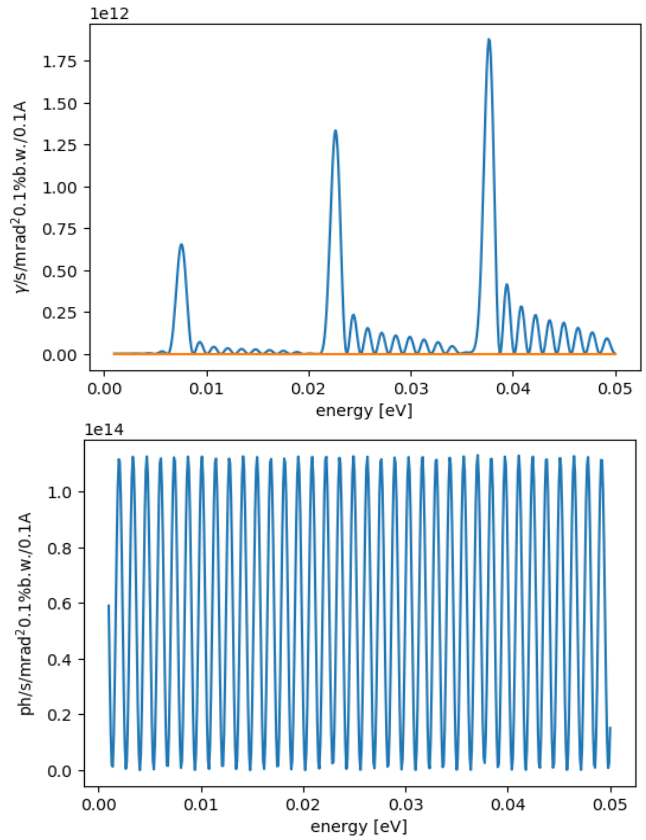

Figure 14: On-axis undulator radiation only (left). Off axis, TUR dominates ($\theta_x = 0.06$mrad, $\theta_y = 0$) (right).

5.4 Undulator Radiation Harmonics

From Fig. 12, one can see the wiggler generates strong harmonics and in fact broad spectrum that is characteristics of bending magnets. This is expected and can be used to our advantage: we don't have to tune the undulator K very much and can place the bandwidth filter at any frequency between 3-20 THz to obtain THz radiation at 100 uJ level. One must note that the transverse profile of the higher harmonics (e.g., the second harmonic) may be not as good as the fundamental frequency.

6 References

[1] A High-Power, High-Repetition Rate THz Source for Pump-Probe Experiments at LCLS-II, Z. Zhang et al., JSR 2020.